JOURNAL OF MATERIALS SCIENCE 23 (1988) 2479-2484

Effect of inclusion content on the creep rupture properties of type 17Cr–8Ni–2Mo weld metals

B. A. SENIOR
Technology Planning and Research Division, Central Electricity Generating Board, Central Electricity Research Laboratories, Kelvin Avenue, Leatherhead, Surrey KT22 7SE, UK

It has been known for some time that austenitic weldments exhibit low and variable creep rupture properties, but many of the factors controlling these properties are not well understood. In this investigation, two welds (Type 316) with similar compositions and fabricated using the same welding parameters, but with different electrode coatings, have been examined after creep testing. The results indicate that the inclusion and silicon content of type 316 welds can strongly influence their creep rupture properties, a high inclusion density being associated with poor creep rupture properties, and a low silicon content with a higher creep rate. This has been explained with reference to the micromechanism of creep failure operating in these welds.

1. Introduction

AISI type 316 austenitic stainless steel has found considerable application in both conventional and nuclear power plants. Considerable variability in the creep rupture properties of wrought and weld metals for type 316 material exists, however. A recent assessment of available data relating to wrought type 316 material suggested an optimum composition containing a low carbon and intermediate nitrogen content [1]. A similar specification has been adopted for nuclear applications in France [2], preliminary work suggesting improved creep properties and good ductility are associated with this type of material.

With the introduction of such materials, it is increasingly recognized that the limiting aspect of a type 316 structure is now likely to be the weld. Some reasons for the large scatter in creep rupture data relating to type 316 welds have been identified, including precipitate type and density [3], residual elements [4], ferrite content [5] and morphology [6], but many areas of uncertainty still exist. In particular, the effects of electrode coating on creep rupture properties are still not fully understood. In the present investigation the interrelationships between creep rupture properties and microstructure of type 17Cr–8Ni–2Mo weldments fabricated using basic and rutile coatings are examined, and effects on the micromechanism of failure are used to explain the observed creep properties.

2. Experimental procedure

2.1. Materials

Type 316 plate-to-plate butt welds, each approximately 76 × 15 × 2 cm^3, were deposited using the manual metal arc process along a 76 cm long single U groove. A total of 13 weld runs were used to complete the weld, the bulk of the weld metal being deposited with 5 mm electrodes. Smaller electrodes were used near the root of the weld. Two electrode types were used, weld A having a basic electrode coating and weld B a rutile electrode coating. The bulk chemical compositions of the weldments examined are given in Table I, together with chromium and nickel equivalents, calculated according to Hammar and Svensson [7]. Oxygen levels for these weld metals were obtained using the vacuum fusion technique [8], and are included in Table I.

2.2. Creep rupture testing

Creep rupture testing at 600° C and 650° C was carried out by the Electrical Research Association using two specimen orientations, longitudinal to the weld and cross weld. Specimens from weld A (longitudinal) tested at 600° C, 201 MPa for 228 h (A1) and weld B (longitudinal) tested at 600° C, 201 MPa for 7860 h (B1) were examined in detail this investigation, other specimens being subject to less rigorous examination. The gauge length of the specimens was 45 mm, with a diameter of 11 mm. This non-standard specimen geometry was adopted following work which demonstrated that considerable scatter in creep rupture properties can arise if several weld beads are not sampled within the specimen diameter [9].

2.3. Microstructural characterization

Following creep rupture testing, samples from the grip and gauge length of precrept specimens were prepared for optical examination using standard metallographic techniques. When necessary, specimens were etched electrolytically in 10% HCl/methanol. Samples from the gauge length and grip were also taken for X-ray analysis using the technique developed by Chung [10] and applied to austenitic steels by Lai and Galbraith [11].

2.3.1. Ferrite measurement

The residual ferrite levels in the weld metals were

0022–2461/88 $03.00 + .12

TABLE I Bulk composition and equivalents of the weldments used

Weld	wt %								
	C	Cr	Co	Cu	Mn	Mo	Ni	Nb	P
A	0.055	18.1	0.06	0.06	1.9	1.7	9.4	<0.1	0.016
B	0.069	17.3	0.03	0.06	1.89	2.0	9.4	<0.1	0.017

Weld	wt %					Hammar and Svensson equivalents		0 wt %
	Si	S	V	N	B	Cr_{eq}	Ni_{eq}	
A	0.27	0.007	0.055	0.037	0.0006	20.83	11.78	0.070
B	0.40	0.005	0.076	0.037	0.0003	20.64	12.09	0.047

measured directly using a Ferritscope, which is a magneto-inductive device calibrated in percentage ferrite against a series of standards. Since the ferrite content may vary considerably within a multipass weldment [12], the mean of six readings in mutually perpendicular directions was taken.

2.3.2. Inclusion content

The inclusion content of the welds was assessed using polished samples taken from the grip of precrept specimens. A series of thirty fields was analysed on two samples from each weld metal, at a magnification of X500, using a Quantimet image analysis system. This gave a total area examined of 12×10^4 μm^2 with a resolution of 0.2 μm or better. Fields were chosen in a random manner, where possible traversing several weld beads.

Data relating to the composition of inclusions present were obtained using energy dispersive X-ray (EDX) spectroscopic analysis of inclusions extracted onto carbon replicas, and examined in a Hitachi H700H transmission electron microscope (TEM) with scanning (STEM) capability. Larger inclusions were analysed on polished sections using a high resolution scanning electron microscope (SEM) with EDX analytical facilities.

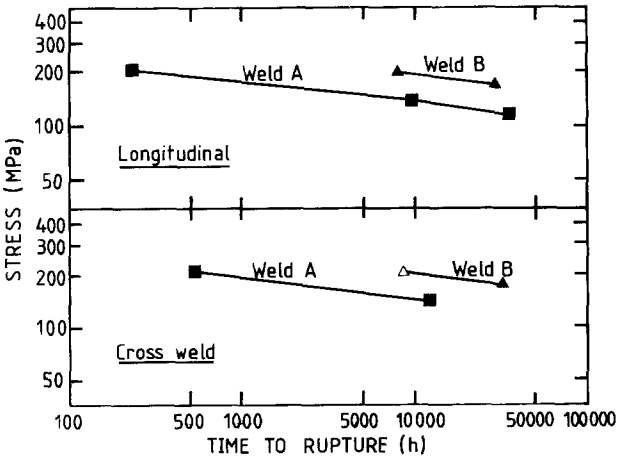

Figure 1 Creep rupture curves for the two weldments used in this investigation. The open symbol denotes fracture outside the weld region.

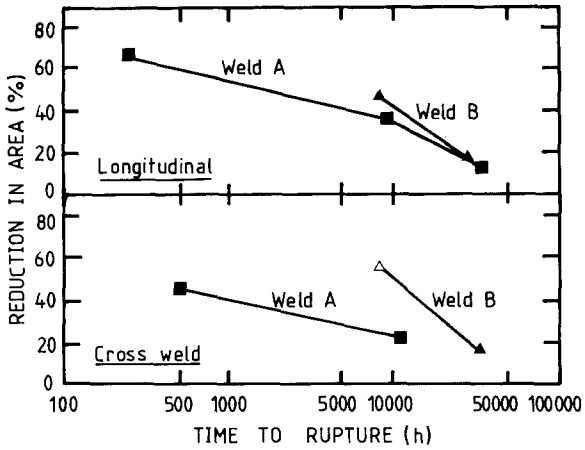

Figure 2 Creep ductility data for the two weldments used in this investigation. The open symbol denotes fracture outside the weld region.

2.3.3. Precipitate analysis

The precipitates formed during creep testing were analysed on carbon extraction replicas, prepared from polished and lightly etched surfaces. Extracted particles were analysed using EDX analysis in the Hitachi H700H (STEM mode), at an accelerating voltage of 200 kV and magnifications of × 50 000 and × 100 000. Analysis conditions gave count rates in the range 800–3000 c.p.s. The crystal structures of the precipitates present were identified by comparing EDX spectra with calibrated spectra for type 316 material (e.g. [13], [14]).

2.4. Post test metallography

In order to investigate the extent of creep damage and the mode of creep failure, samples taken from the gauge length of precrept specimens were examined for cavitation and cracking. Low magnification examination using optical microscopy was performed on polished sections (etched and unetched). In addition, sections were lightly etched and examined in a Hitachi S800 high resolution SEM.

3. Results

3.1. Creep rupture testing

Fig. 1 shows creep rupture data for welds A and B, tested at 600° C. Data from tests at 650° C are not sufficient for results to be included here, and Table II shows data at this temperature. It is evident from Fig. 1 that the creep rupture strength of weld A is considerably lower than that of weld B. Creep ductility results are summarized in Fig. 2 and show that the lower creep rupture strength of weld A is associated with lower creep ductility, although the ductilities are comparable after longer term testing.

TABLE II Creep rupture data for the welds used in this investigation. Longitudinal specimens tested at 650° C

Weld	Stress ($MN m^{-2}$)	Rupture life (h)	Reduction in area (%)
A	108	2 300	27
	77	14 544	7
B	108	11 508	5
	77	29 436	1

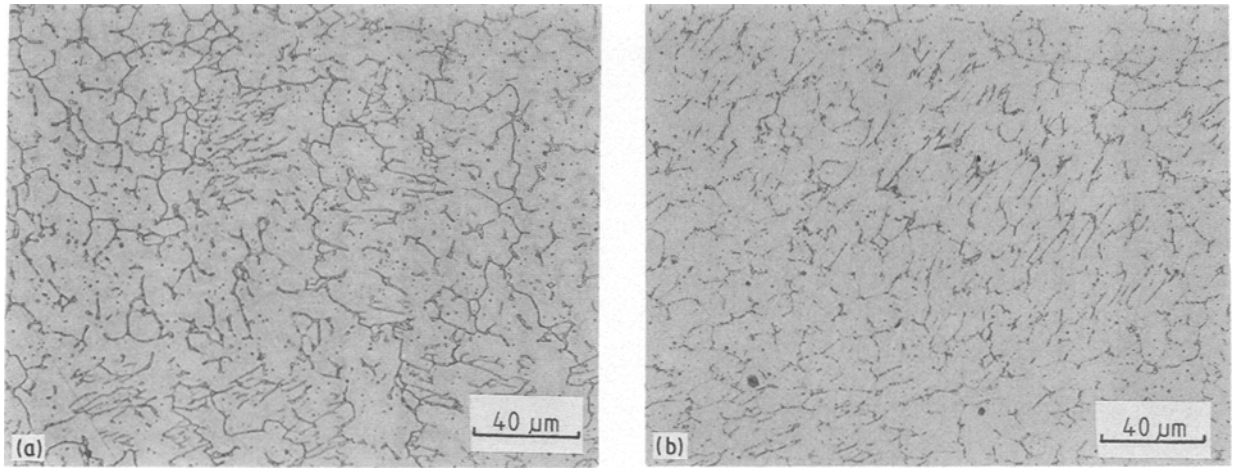

Figure 3 Optical microstructure of (a) weld A and (b) weld B, sectioned perpendicular to the welding direction.

3.2. Microstructural characterization

3.2.1. Optical examination

The microstructure of the welds was examined on sections taken parallel and perpendicular to the welding direction, and examples of the observed microstructure following creep testing are shown in Fig. 3.

The results obtained indicate that solidification has occurred principally as primary ferrite, with some austenite formation from the last of the melt to solidify. This is associated with nickel depletion and chromium enrichment at the cores of the cellular dendrites [15–17]. The formation of austenite continues in the solidified weld by the $\delta \rightarrow \gamma$ transformation, although the most stable ferrite (i.e. that which solidified first and is the most enriched in chromium equivalent elements) is retained. The vermicular form of ferrite, shown in Fig. 3a, is characteristic of primary ferritic solidification. Optical examination of several fields showed that the transformation products in these welds do not form a continuous network, of the type expected when original ferrite levels exceed 7–10% [12, 18].

3.2.2. Ferrite content

The measured ferrite levels in specimens cut from the gauge length and grip of A1 and B1 are given in Table III, together with measured values for the initial weldments. Data indicate that ferrite transformation has occurred more extensively in sample B1, a result which is consistent with the greater duration of this test.

The results given in Table III also show that ferrite transformation has occurred more rapidly in the gauge length than in the grip. This is almost certainly a consequence of the rapid diffusion rates associated with high dislocation densities during deformation.

3.2.3. Inclusion content

Both of the weld metals were found to contain a large number of inclusions. Results from quantitative measurement of the inclusion content are summarized in Table IV.

It is evident from these results that the size and shape distributions of inclusions in these weldments are similar, but that weld A contains approximately twice the number of inclusions present in weld B. The higher inclusion density in weld A is associated with a higher oxygen content (Table I).

EDX analysis of extracted inclusions showed that these were predominantly manganese silicate particles. A small number of spinel type inclusions were also observed.

3.2.4. Precipitate analysis

3.2.4.1. Bulk extraction. Results from the X-ray analysis of bulk extracted precipitates are summarized in Table V. The accuracy of the technique is limited to $\pm 5\%$ of quoted values, the sensitivity of the technique being strongly dependent upon the possibility of overlap.

Data given in Table V show that the total weight fraction of precipitates in B1 is almost 100% greater than in A1, irrespective of position within the creep specimen, for similar amounts of weld metal dissolved. This difference is consistent with the increased test duration of B1. The detection of sigma phase in A1 (gauge length) but not in B1 using this technique

TABLE III Measured ferrite content of the as-welded, creep tested and aged samples

Condition	Weld A			Weld B		
	As Welded	Crept ($g l^{-1}$)	Aged (grip)	As Welded	Crept ($g l^{-1}$)	Aged (grip)
% ferrite	6.4	3.38 ± 0.8	4.22 ± 1.3	5.2	1.34 ± 0.3	2.58 ± 0.2

TABLE IV Summary of the inclusion content of the weldments

Material	Mean inclusion diameter (equivalent) (μm)	Number density (m^{-2})	Mean aspect ratio
Weld A	1.75	6.03×10^{10}	1.27
Weld B	1.42	3.30×10^{10}	1.30

cannot be readily accounted for; EDX analysis of extracted precipitates showed that sigma phase was present in both specimens. It is conceivable that partial dissolution of this phase may occur in type 316 material after long etching times in 10% HCl/methanol.

3.2.4.2. STEM/EDX microanalysis. Examination and analysis of the precipitates present showed that only σ, $M_{23}C_6$ and Laves' type Fe_2Mo phase were present in these specimens. The morphology of precipitates in A1 and B1 was not similar, as Fig. 4 shows. A1 contained relatively large $M_{23}C_6$ precipitates and sigma particles in prior ferrite morphologies and a fine dispersion of $M_{23}C_6$ and Fe_2Mo precipitates present in interferritic regions. The presence of Laves phase has not been widely reported in type 316 weld metals, although its presence in wrought 316 material [13, 14] is now well documented.

More extensive precipitation of Fe_2Mo and small $M_{23}C_6$ carbides was observed in B1, with large $M_{23}C_6$ and σ precipitates also present. Detection of Laves' phase using bulk X-ray extraction techniques was not possible, since its major X-ray peaks overlap with large $M_{23}C_6$ and σ phase peaks.

3.3. Post test metallography

Optical examination of polished sections revealed extensive cavitation at inclusions, in the gauge length of both A1 and B1. A small number of cracks were observed in B1, crack propagation having occurred perpendicular to the tensile axis.

Examination of lightly etched sections in the SEM confirmed the presence of cavities at inclusions (Fig. 5), and at precipitates (Fig. 6). Cavitation was more extensive in B1, and EDX analysis of cavitated precipitates showed that sigma and $M_{23}C_6$ particles, associated with prior ferrite, had acted as nucleation sites for cavities.

TABLE V Summary of the results from bulk extraction analysis of precipitates present

Weld type	Specimen	Position	Weight %	
			$M_{23}C_6$	σ
Weld A	A1	Gauge length	0.96	0.19
		grip	0.98	—
Weld B	B1	Gauge length	1.95	—
		grip	1.63	—

4. Discussion

4.1. Creep rupture mechanism

The mechanisms of creep failure in type 316 weld metal are limited by the absence of an equiaxed grain structure, and the presence of ferrite. Thomas [5] has shown that the mechanism of failure is strongly dependent upon the ferrite content of the weld. In low ferrite (0.5%) and fully austenitic welds, wedge cracking occurs along columnar grain boundaries. When ferrite levels exceed 1–2%, however, cavity formation occurs at ferrite/austenite, carbide/austenite and intermetallic/austenite boundaries, in addition to intermetallic phase cracking [19, 20]. The present investigation has demonstrated that cavities had formed in A1 and B1 as a result of $M_{23}C_6$/austenite interface decohesion, manganese silicate/austenite interface decohesion and cracking of spinel-type inclusions, sigma and sigma/austenite interfaces. Coalescence of the cavities formed at carbides and sigma gave rise to small cracks, which could propagate rapidly along the weak interphase boundaries.

In weldments where the ferrite network is largely continuous, crack propagation may then continue across the specimen along the interphase boundaries. Since these boundaries are weak, crack propagation occurs very much more rapidly than the continuing cavitation process, and the creep rupture life is consequently low [5, 19].

In the welds used in this study, the network of ferrite and transformation products was not continuous. There is consequently no easy path

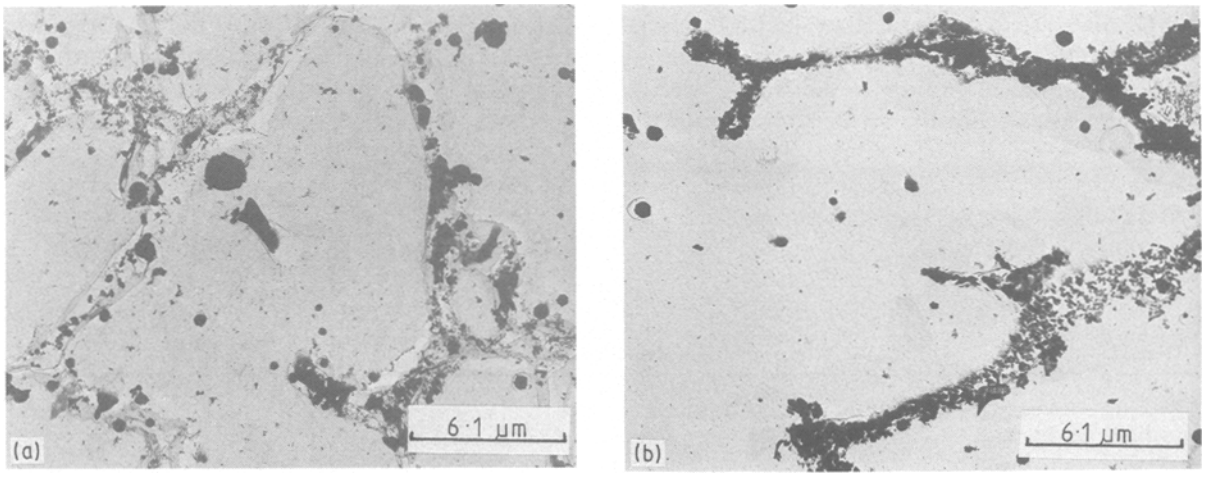

Figure 4 Precipitates extracted from (a) specimen A1 and (b) specimen B1 (gauge length), showing the distribution of precipitated phases.

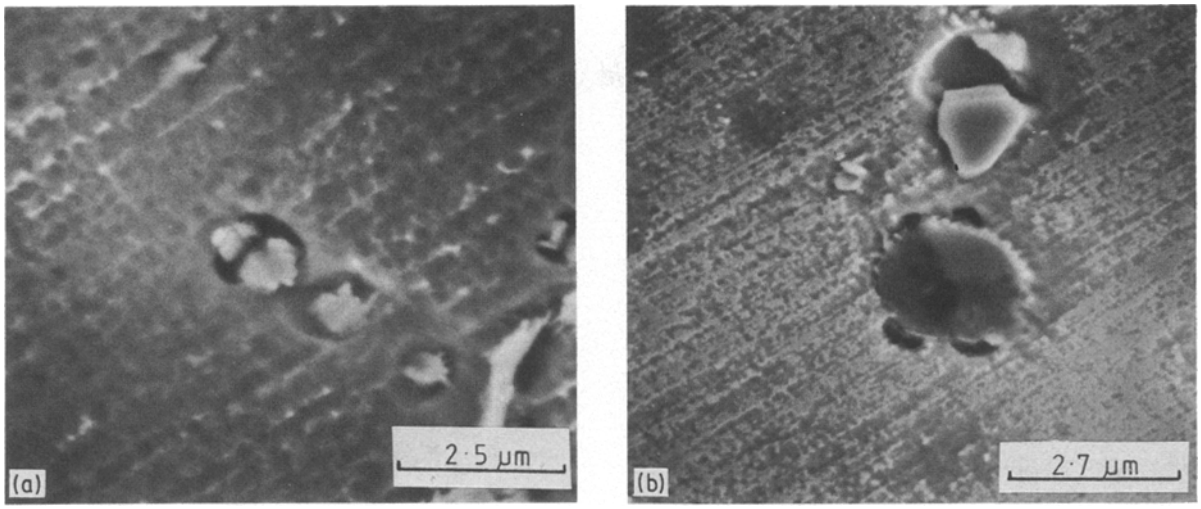

Figure 5 Examples of cavity nucleation at inclusions by (a) fracture of a spinel-type inclusion (b) interfacial decohesion at a manganese silicate inclusion.

through the austenite when the crack has propagated along an interphase boundary, and several small cracks may be formed in this manner during creep testing, as observed on sections of B1.

There is little precipitation within the austenite matrix in these specimens (Fig. 4) and, in the absence of a favourably oriented columnar grain boundary, the crack propagation mechanism which can readily operate is coalescence with inclusion nucleated cavities at the crack tip. The growth and coalescence of voids ahead of a blunting crack tip is determined by the distance between the void and the crack tip [21], and crack propagation through A1, which has a high inclusion density, is consequently rapid. B1 contains a lower density of inclusions, and crack propagation is therefore slower in this specimen. This results in a longer test duration, greater ductility and the presence of several small cracks, formed perpendicular to the tensile axis. It should be noted that more extensive cavitation was present in B1 than in A1, a result which supports the conclusion that a more rapid cavitation rate in A1 was not primarily responsible for the observed differences in creep rupture properties.

4.2. Creep rupture ductility

The results presented in Figs 1 and 2 show that changes in creep rupture strength are not always associated with marked reductions in the creep ductility of these welds. This implies that the creep rate of these weldments is different in shorter term tests. The precipitates present within the two weldments were similar, with no evidence for extensive precipitation hardening by stable trace element (titanium, vanadium, niobium) carbides, and the difference in creep rate may, therefore, be attributable to solid solution hardening. Table I shows that of the elements analysed the only major compositional differences are in silicon and carbon content. Carbon is known to strengthen austenite, and is present in both the weld metals examined as $M_{23}C_6$ and, since the solubility of carbon in this type of steel is 0.0004 wt % at 600° C [22], in the matrix also. The results shown in Table V indicate that the precipitation of $M_{23}C_6$ in specimen B1 is close to equilibrium (i.e. free carbon is ~ 0.0004 wt %), but that approximately 0.005 wt % carbon is not present in A1 as $M_{23}C_6$, assuming the carbide composition is close to $Cr_{16}Fe_5Mo_2C_6$ [23]. In

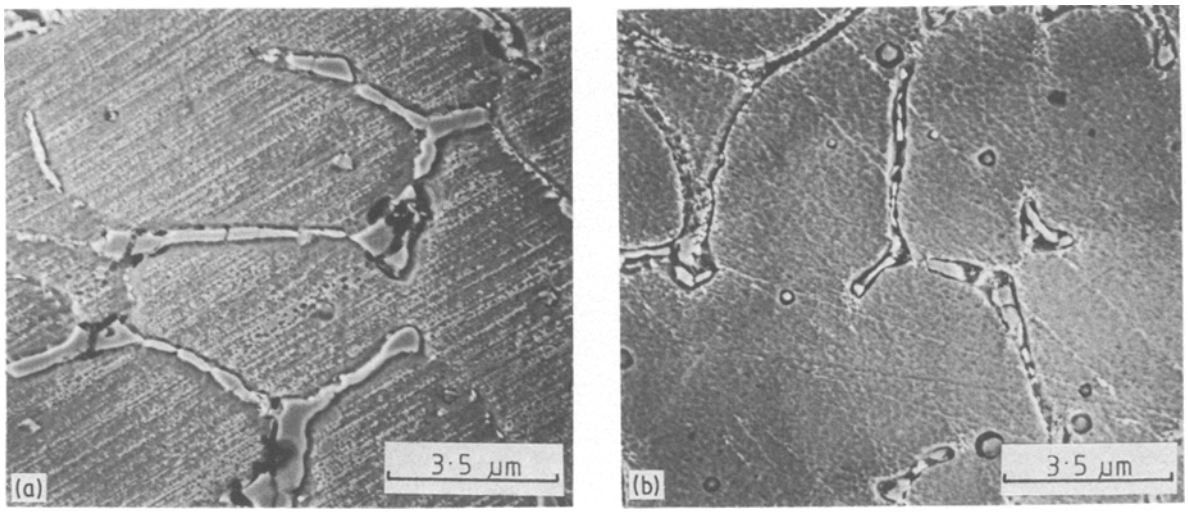

Figure 6 Cavitation at $M_{23}C_6$ and sigma phase transformation products in (a) specimen A1 and (b) specimen B1.

the absence of other carbides, therefore, consideration of matrix strengthening by free carbon suggests that the creep rate of A1 should be lower than the creep rate of B1. The creep rupture data shown in Figs 1 and 2 show a reverse trend, however, the creep rate of B1 being lower than that of A1.

A second compositional difference is in silicon content, an element which is also known to impede dislocation motion and hence strengthen austenite. Weld A contains 0.27 wt % Si, and weld B contains 0.40 wt % Si. This difference is enhanced by the relatively high volume fraction of manganese silicate inclusions present in weld A, which further reduces the matrix silicon content. An approximate calculation of the residual silicon present in the matrix, using measured inclusion data and assuming that all inclusions have a composition of $MnO.SiO_2$ (Section 3) gives values of 0.21 wt % Si (weld A) and 0.38 wt % Si (weld B). These results are consistent with work on type 308 weld metals [24] in which lower silicon contents were associated with higher creep rates. This may increase the rate at which cavitation and crack propagation occurs, in addition to increasing the creep ductility of weld A. It should be noted, however, that the long term ductility of the weldments is comparable, suggesting that the difference in matrix strength is reduced as the test duration exceeds 10 000–20 000 h. This result is not incompatible with a mechanism of solid solution strengthening by silicon since extensive precipitation of Fe_2Mo (which contains up to 15 wt % Si) will reduce the matrix silicon content in long term tests. Fig. 1 indicates, however, that the creep rupture strength difference is maintained in tests greater than 30 000 h, suggesting that the microstructural changes discussed above have little effect on the creep rupture strength, the higher inclusion content of weld A resulting in lower creep strength irrespective of test duration.

The high oxygen and hence inclusion content of the basic coated weld metal (A) relative to the rutile coated weld metal (B) is a consequence of several features, not all of which are understood. The complexity of flux formulations, and the fact that weld metal–slag reactions do not generally proceed to equilibrium, restricts the understanding of weld pool chemistry. Factors such as oxygen content cannot, therefore, be readily predicted even when details of the flux formulations are available.

5. Conclusions

The inclusion content of austenitic type 316 weldments influences their creep rupture properties, when the solidification structure contains 5.0–6.5% ferrite.

The creep failure process operating is cavitation at interphase boundaries, followed by crack propagation along these boundaries. When the inclusion density is high, propagation may continue through the specimen by coalescence of the crack tip with inclusion nucleated voids. When the inclusion content is lower, more extensive deformation is necessary before failure of the specimen occurs.

A relatively low matrix silicon content leads to higher creep rates, which may enhance the rate at which cavitation and crack propagation occurs.

Acknowledgements

The author would like to thank Mr A. Chowdhury for his assistance in specimen preparation, and Mr I. Pearce for performing the X-ray analysis of extracted precipitates. This work was carried out at the Central Electricity Research Laboratories and is published by permission of the Central Electricity Generating Board. Creep-rupture data and tested specimens were supplied by the Electrical Research Association.

References

1. J. K. L. LAI, *J. Nucl. Mater.* **99** (1981) 148.
2. P. RABBE and J. HERITIER ASTM STP 679, edited by C. R. Brinkman and H. W. Garvin (American Society for Testing and Materials, Philadelphia 1979) p. 124.
3. C. A. P. HORTON, P. MARSHALL and R. G. THOMAS, in Proceedings of the International Conference "Mechanical Behaviour and Nuclear Applications of Stainless Steel at Elevated Temperatures", Varese, Italy, May, 1981 (Metals Society, London, 1982) p. 66.
4. R. L. KLUEH and D. P. EDMONDS, *Weld. J.* **65** (1986) 156s.
5. R. G. THOMAS, *Weld. J. Res. Suppl.* **58** (1978) 81.
6. J. K. L. LAI, B. NATH, R. TOWNSEND and D. S. WOOD, In Proceedings of the International Conference "Welding and Fabrication in the Nuclear Industry", BNES, London, April 1979, Paper No 30.
7. O. HAMMAR and V. SVENSSON, "Solidification and Casting of Metals", (Metals Society, London, 1979) p. 401.
8. T. J. WEBBER and C. J. PICKFORD, unpublished research.
9. C. A. P. HORTON and J. K. L. LAI, *Met. Sci.* Oct **14** (1980) 502.
10. F. H. CHUNG, in Proceedings of the 22nd Annual Conference on Applied X-Ray Analysis "Advances in X-ray Analysis Vol. 17", Denver, August 1973 (Plenum Press, N.Y., 1974).
11. J. K. L. LAI and I. F. GALBRAITH, *J. Mater. Sci.* **15** (1980) 1297.
12. W. T. DeLONG, *Weld. J.* **53** (1974) 273.
13. L. P. STOTER, *J. Mater. Sci.* **16** (1981) 1039.
14. B. WEISS, C. W. HUGHES and R. STICKLER, *Prac. Metallog.* **VIII** (1971) 528.
15. J. A. BROOKS, J. C. WILLIAMS and A. W. THOMPSON, *Met. Trans.* **14A** (1983) 1271.
16. *Idem ibid.* **14A** (1983) 23.
17. M. J. CIESLAK, A. M. RITTER and W. F. SAVAGE, *Weld. J.* **61** (1982) 1.
18. A. M. HORSFIELD, *Stainless Steel Ind.* **11** (1983) 8, 9, 17.
19. R. G. THOMAS, R. D. NICHOLSON and R. A. FARRAR, *Met. Technol.* **11** (1984) 61.
20. J. K. L. LAI and J. R. HAIGH, *Weld. J.* **58** (1979) 13.
21. N. ARAVAS and R. M. McMEEKING, *J. Mech. Phys. Sol.* **33** (1985) 25.
22. M. DEIGHTON, *J. Iron Steel Inst.* **208** (1970) 1012.
23. D. R. HARRIES, in Proceedings of the International Conference "Mechanical Behaviour and Nuclear Applications of Stainless Steels at Elevated Temperatures", Varese, Italy, May 1980 (Metals Society, London, 1981) p. 1.
24. R. W. SWINDEMAN, V. K. SIKKA and R. L. KLUEH, *Met. Trans.* **14A** (1983) 581.

Received 25 June
and accepted 16 December 1987